ACS OMEGA

Open Access

http://pubs.acs.org/journal/acsodf

Article

A Series of Endohedral Metallo-BN Fullerene Superatomic Structures

Jia Wang,* Huanming Zhang, Meiqi Wang, and Wanyi Zhang

Cite This: *ACS Omega* 2024, 9, 27748−27753

Read Online

ACCESS | Metrics & More | Article Recommendations | Supporting Information

ABSTRACT: Superatoms are crucial in the assembly of functional and optoelectronic materials. This study investigates the endohedral metallo-boron nitride [boron nitride (BN)] fullerenes $U@B_{12}N_{12}$, $Cm@B_{12}N_{12}$, and $U@B_{16}N_{16}$ in theory. Our findings confirm that $U@B_{12}N_{12}$, $Cm@B_{12}N_{12}$, and $U@B_{16}N_{16}$ are superatoms and their electronic configurations are $1P^61S^21D^{10}1F^{14}2P^62S^22D^{10}2F^{12}3P^6$, $1P^61S^21D^{10}1F^{14}1G^{16}1H^{16}2S^22P^62D^{10}2F^{12}$, and $1P^61S^21D^{10}1F^{14}2P^62S^22D^{10}2F^{14}$, respectively. Notably, the orbital energy levels in these superatoms exhibit a flipping phenomenon, deviating from those of previous superatom studies. Further, the orbital composition analyses reveal that superatomic orbitals 1S, 1P, 1D, and 1F mainly originate from BN cages, whereas the 2S, 2P, 2D, 2F, and 3P superatomic orbitals arise from hybridizations between BN cage orbitals and the 7s, 7p, 6d, and 5f orbitals of actinide atoms. And the energy gap of endohedral metallo-BN fullerene superatoms is reduced by introducing actinide atoms. Additionally, the analyses of ionization potentials and electron affinities show that $U@B_{12}N_{12}$, $Cm@B_{12}N_{12}$, and $U@B_{16}N_{16}$ have lower ionization potentials and higher electron affinities, suggesting decreased stability compared to that of pure BN cages. This instability may be linked to the observed flipping of the superatomic orbital energy levels. These insights introduce new members to the superatom family and offer new building blocks for the design of nanoscale materials with tailored properties.

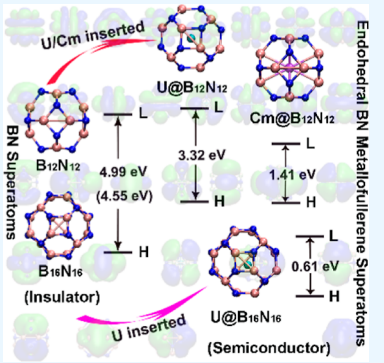

INTRODUCTION

Endohedral metallofullerenes (EMFs) are prominent in various potential applications such as electricity, optics,[1] biomedicine,[2−4] superconductors, ferroelectric materials,[5,6] and nanomaterials.[7] Clusters with embedded atoms or small molecules form stable core@shell systems.[8,9] Specifically, C_{28} clusters demonstrate distinct stability compared to other clusters with an open-shell electronic structure,[10] while research on $M@C_{28}$ (M = Th, Pa^+, U^{2+}, and Pu^{4+}) indicates a significant enhancement in stability through actinide encapsulation.[11−13] Similarly, $[An@Pb_{12}]^n$ (An = Pu, Am, and Cm) clusters are considerably stabilized by the insertion of lanthanide or actinide atoms, benefiting from robust Pb−An interactions due to attractive electrostatic effects and significant orbital interactions.[14]

Superatoms with atomic shell closure have garnered substantial interest due to their inherent stability.[15−18] This interest has catalyzed the emergence of a new field in materials science dedicated to synthesizing novel materials with superatoms as building blocks[19−23] and experimentally observed superatoms with unique mass spectra, such as Na_{40},[16] Al_{13}^-,[24−26] and Au_{20}.[18] Moreover, nonmetallic superatoms like C_{60}[27−30] and B_{40}[31,32] have also been observed experimentally. Although B_{40} is a superatom, it is not a closed-shell electronic structure.[32] However, the studies on $U@B_{40}$ prove that it is a stable closed-shell structure.[9] Recent studies on boron−nitrogen (BN) cages identified that $B_{12}N_{12}$, $B_{16}N_{16}$, and $B_{28}N_{28}$ are nonmetallic superatoms.[33,34] Consequently, we hypothesize that endohedral metallo-BN fullerenes may exhibit greater stability than BN cages alone.

Various BN cages have been experimentally synthesized[35,36] and have garnered significant interest due to their extensive band gaps.[33] And BN clusters have many attractive properties, such as high temperature stability, low dielectric constant, and oxidation resistance.[37,38] Previous studies on Ti-doped BN fullerenes have shown that the externally bound complexes of $Ti(BN)_n$ are strikingly more stable than the endohedral ones.[39] In this work, we constructed $U@B_{12}N_{12}$, $Cm@B_{12}N_{12}$, and $U@B_{16}N_{16}$, and the results show that they are superatoms and their stability is lower than that of BN cages. This observation deviates from earlier research and surpasses initial expectations, presenting new insights into the stability of endohedral metallo-BN fullerenes.

RESULTS AND DISCUSSION

U and Cm atoms are encapsulated within $B_{12}N_{12}$ and $B_{16}N_{16}$ cages to form endohedral metallo-BN fullerenes $U@B_{12}N_{12}$, $Cm@B_{12}N_{12}$, and $U@B_{16}N_{16}$. The structures and electronic properties of these fullerenes have been investigated using density functional theory (DFT) methods.[40] The geometric

Received: May 20, 2024
Revised: June 5, 2024
Accepted: June 7, 2024
Published: June 12, 2024

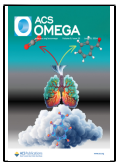

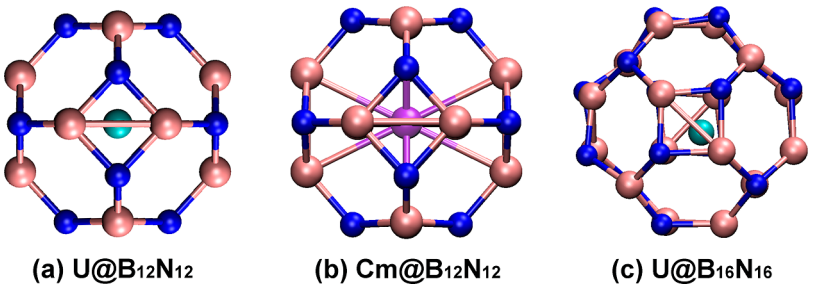

Figure 1. Geometric structures diagram. (a) $U@B_{12}N_{12}$, (b) $Cm@B_{12}N_{12}$, and (c) $U@B_{16}N_{16}$; the pink, blue, cyan, and purple atoms in the structures represent B, N, U, and Cm atoms, respectively.

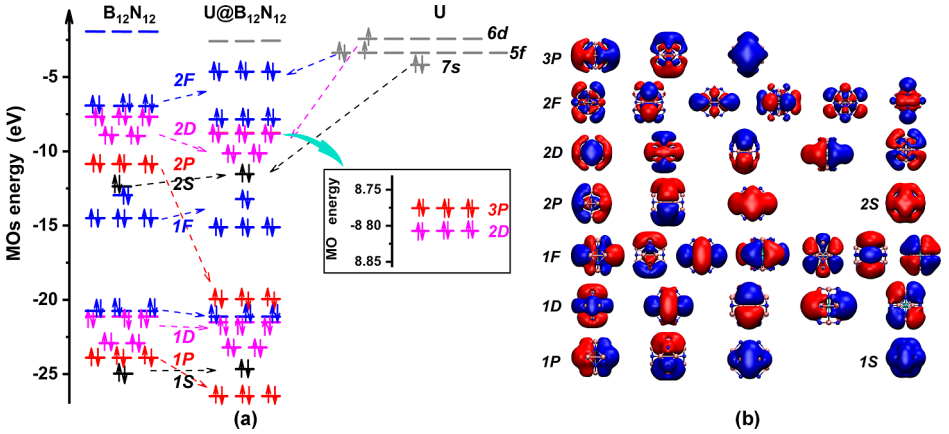

Figure 2. Superatomic orbitals and energy levels for $U@B_{12}N_{12}$ at the PBE level. (a) Superatomic orbital energy levels and (b) superatomic orbitals. S, P, D, and F represent superatomic orbitals of $U@B_{12}N_{12}$, respectively.

structures calculated at the PBE/TZ2P level are shown in Figure 1. In the $U@B_{12}N_{12}$ and $Cm@B_{12}N_{12}$ configurations, the U and Cm atoms are centrally positioned within the cages. However, in the $U@B_{16}N_{16}$ fullerene, the U atom is offset from the center, which is attributed to the larger diameter of the $B_{16}N_{16}$ cage. The calculated results show that the ground state of $U@B_{12}N_{12}$ is a singlet. The energy difference between the triplet and the ground state is 1.45 eV, and the energy difference between the quintet and the ground state is 3.07 eV. Similarly, the ground state of $U@B_{16}N_{16}$ is a singlet, and the energy differences between the ground state and the triplet or quintet are 0.42 and 1.61 eV, respectively. However, the ground state of $Cm@B_{12}N_{12}$ is a quintet, and the energy differences between the ground state and the singlet or triplet are 1.40 and 0.98 eV, respectively. Detailed bond energies are provided in Table S1 of the Supporting Information.

The electronic properties of $U@B_{12}N_{12}$, $Cm@B_{12}N_{12}$, and $U@B_{16}N_{16}$ are thoroughly analyzed. The molecular orbitals (MOs) of $U@B_{12}N_{12}$, displayed in Figure 2, span an energy range from −26 to −12.5 eV. The MO of $U@B_{12}N_{12}$ resembles an s-like atomic orbital, identified as the 1S superatomic orbital. 1P superatomic orbitals contain triple degenerate p-like atomic orbitals, while 1D superatomic orbitals consist of both double and triple degenerate d-like atomic orbitals. Additionally, seven f-like orbitals, including two triple degenerate orbitals and one nondegenerate orbital, form the 1F superatomic orbitals. Notably, the 1S, 1P, 1D, and 1F superatomic orbitals predominantly consist of $B_{12}N_{12}$ cages [as shown in Figure 2b], which are consistent with $B_{12}N_{12}$.[34]

Within the energy level range of −20 to −4 eV, s-, p-, d-, and f-like atomic orbitals are also present, referred to as superatomic orbitals 2S, 2P, 2D, and 2F with the "principal quantum number" of 2, respectively. The orbital structure includes one 2S, three 2P, and five 2D superatomic orbitals, with six double-occupied 2F superatomic orbitals. Despite the 2F electronic shell not being fully filled, three higher angular momentum 3P superatomic orbitals are observed (as highlighted in the inset of Figure 2), which are different from previously studied superatoms.[9,32,34] Thus, the electronic configuration of $U@B_{12}N_{12}$ is $1P^61S^21D^{10}1F^{14}2P^62S^22D^{10}2F^{12}3P^6$. The superatomic orbitals 2S, 2P, 2D, 2F, and 3P result from hybridization of the 7s, 7p, 6d, and 5f orbitals of the U atom with the MOs of the $B_{12}N_{12}$ cage. However, contrary to typical atomic orbital energy levels, the energy of 1P or 2P superatomic orbitals is lower than that of the 1S or 2S superatomic orbitals for $U@B_{12}N_{12}$. Thus, the insertion of U atoms in the $B_{12}N_{12}$ cage leads to an inversion of the MO energy. This phenomenon is different from that of other superatoms such as $U@B_{40}$,[9] $U@C_{28}$,[8] and $An@Au_{14}$ (An = Ac, Tu, and Pa).[41]

We examined the atomic orbital composition of each superatomic orbital, as shown in Figure 3. In the figure, red indicates the contribution of 2s atomic orbitals, while blue signifies the contribution of 2p atomic orbitals. The superatomic orbitals 1S, 1P, and 1D and some of the 1F orbitals are predominantly composed of the 2s atomic orbitals from B and N atoms in the BN cages. And the contributions to the remaining 1F, 2S, 2P, 2D, and 2F superatomic orbitals primarily arise from the 2p atomic orbitals of B and N atoms in the $B_{12}N_{12}$ cage.

The ground state of $Cm@B_{12}N_{12}$ is a quintet with four single occupied electrons, and the spin orientations are

https://doi.org/10.1021/acsomega.4c04765
ACS Omega 2024, 9, 27748−27753

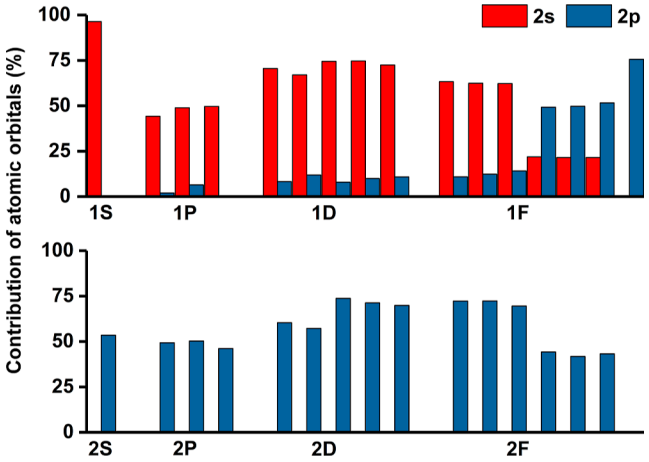

Figure 3. Contributions of the $B_{12}N_{12}$ cage to superatomic orbitals for $U@B_{12}N_{12}$. Red represents the contribution of 2s atomic orbitals and blue denotes the contribution of 2p atomic orbitals.

specified for the Cm and N atoms (spin-up) and B atoms (spin-down), as illustrated in the spin density diagram (Figure S1 in the Supporting Information). Further, analysis of the superatomic orbitals of $Cm@B_{12}N_{12}$ reveals that the superatomic shells 1S, 1P, 1D, and 1F are fully filled. Notably, the energy of 1P superatomic orbitals is lower than that of the 1S superatomic orbitals, a characteristic also observed in $U@B_{12}N_{12}$. The ground state of the Cm atom itself is a nonet with an electronic configuration of $5f^7 6d^1 7s^2$. This electronic configuration contributes to the presence of higher angular momentum superatomic orbitals, such as 1G and 1H, as detailed in Figure S2 in the Supporting Information. The 2S, 2P, and 2D superatomic shells are also fully filled, while 2F superatomic orbitals are partially occupied, as shown in Figure 4. The MO energy levels indicate that the energies of the 2P

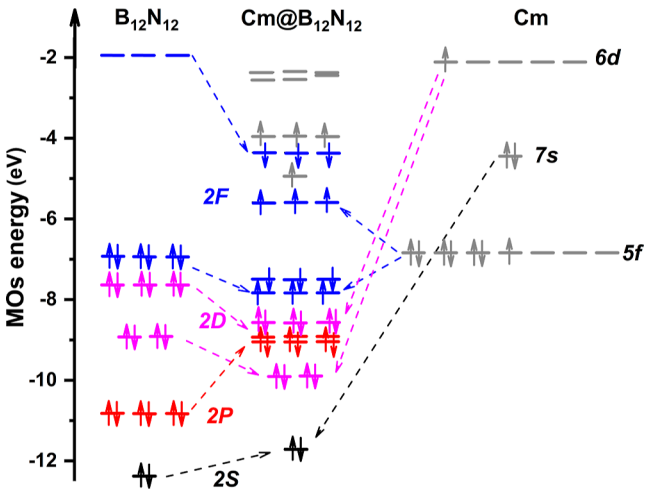

Figure 4. MO energy levels ranging from −12 to −4 eV for $Cm@B_{12}N_{12}$ at the PBE level of theory.

superatomic MOs are higher than those of the doubly degenerate 2D MOs. The electronic configuration of $Cm@B_{12}N_{12}$ is thus given as $1P^6 1S^2 1D^{10} 1F^{14} 1G^{16} 1H^{16} 2S^2 2P^6 2D^{10} 2F^{12}$. Similar to $U@B_{12}N_{12}$, the superatomic orbitals 1S, 1P, 1D, 1F, 1G, and 1H are contributed by the $B_{12}N_{12}$ cage, as shown in Figure S2. And the orbitals 2S, 2P, 2D, and 2F represent hybridizations of the Cm atom's 7s, 7p, 6d, and 5f orbitals with the MOs of the $B_{12}N_{12}$ cage, as shown in Figure S3 in the Supporting Information.

Furthermore, the ground state of $U@B_{16}N_{16}$ is a nonspin-polarized singlet with all MOs being double-occupied, as detailed in Figure 5. This electronic configuration mirrors the

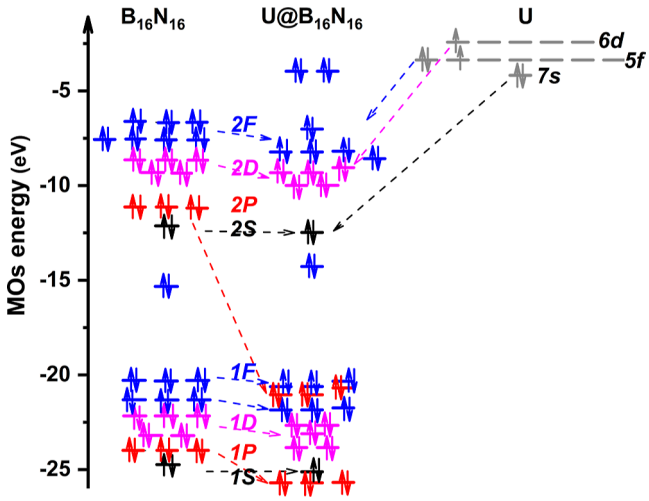

Figure 5. Energy levels for $U@B_{16}N_{16}$, at the PBE level of theory.

fully filled superatomic shells (1S, 1P, 1D, and 1F) found in similar complexes, such as $U@B_{12}N_{12}$ and $Cm@B_{12}N_{12}$. However, unlike in $U@B_{12}N_{12}$ and $Cm@B_{12}N_{12}$, the superatomic shells 2S, 2P, 2D, and 2F in $U@B_{16}N_{16}$ are also fully filled. Consequently, the electronic configuration of $U@B_{16}N_{16}$ is $1P^6 1S^2 1D^{10} 1F^{14} 2P^6 2S^2 2D^{10} 2F^{14}$. The corresponding superatomic orbitals are illustrated in Figure S4 of the Supporting Information. Moreover, akin to the behavior observed in $U@B_{12}N_{12}$, the energy level of 2P superatomic orbitals in $U@B_{16}N_{16}$ is lower than that of the 2S superatomic orbital. This indicates that the incorporation of U atoms into the $B_{16}N_{16}$ cage induces a reversal of the MO energy levels, further demonstrating the unique electronic properties of endohedral metallo-BN fullerenes.

The analysis of the highest occupied MO−lowest unoccupied MO (HOMO−LUMO) gap, which is indicative of chemical stability, reveals that the gaps for $B_{12}N_{12}$ and $B_{16}N_{16}$ are 4.99 and 4.55 eV, respectively. Additionally, the HOMO−LUMO gaps calculated by the PBE/TZ2P functional of $U@B_{12}N_{12}$, $Cm@B_{12}N_{12}$, and $U@B_{16}N_{16}$ are 3.32, 1.41, and 0.61 eV, respectively. This suggests that introducing U and Cm atoms into the $B_{12}N_{12}$ and $B_{16}N_{16}$ cages significantly reduces their HOMO−LUMO gaps. Specifically, $U@B_{12}N_{12}$ demonstrates a higher gap than those of both $Cm@B_{12}N_{12}$ and $U@B_{16}N_{16}$, indicating greater stability for $U@B_{12}N_{12}$. Further calculations with other functionals support these findings. For more detailed discussions, refer to Part 3 in the Supporting Information.

Finally, ionization potentials and electron affinities for endohedral metallo-BN fullerenes $U@B_{12}N_{12}$, $Cm@B_{12}N_{12}$ and $U@B_{16}N_{16}$, as well as for the $B_{16}N_{16}$ cage, are thoroughly analyzed. Bond energies for optimized charged structures are presented in Tables S2 and S3 of the Supporting Information. The vertical ionization potential (VIP) and adiabatic ionization potential (AIP) for $U@B_{12}N_{12}$ are 6.69 and 6.68 eV, respectively. For $Cm@B_{12}N_{12}$, these values are 6.20 and 6.18

https://doi.org/10.1021/acsomega.4c04765
ACS Omega 2024, 9, 27748−27753

eV, respectively, while for $U@B_{16}N_{16}$, both the VIP and AIP are 5.43 eV, as listed in Table 1. Additionally, the vertical

Table 1. VIP, AIP, VEA, and AEA for $U@B_{12}N_{12}$, $Cm@B_{12}N_{12}$, $U@B_{16}N_{16}$, and $B_{16}N_{16}$, at the PBE/TZ2P Level[a]

structures	E_{VIP}	E_{AIP}	E_{VEA}	E_{AEA}
$U@B_{12}N_{12}$	6.69	6.68	0.82	0.84
$Cm@B_{12}N_{12}$	6.20	6.18	0.83	0.83
$U@B_{16}N_{16}$	5.43	5.43	1.43	1.43
$B_{16}N_{16}$	8.76	8.81	0.48	0.68

[a]Units: eV.

electron affinity (VEA) and adiabatic electron affinity (AEA) for $U@B_{12}N_{12}$ and $Cm@B_{12}N_{12}$ are 0.82, 0.84, 0.83, and 0.83 eV and those for $U@B_{16}N_{16}$ are 1.43 and 1.43 eV, respectively. In comparison, the VIP, AIP, VEA, and AEA for $B_{16}N_{16}$ are 8.76, 8.81, 0.48, and 0.68 eV, respectively. The analysis indicates that the ionization potentials for $U@B_{12}N_{12}$, $Cm@B_{12}N_{12}$, and $U@B_{16}N_{16}$ are lower than those of $B_{16}N_{16}$, while their electron affinities are higher. This suggests that $U@B_{12}N_{12}$, $Cm@B_{12}N_{12}$, and $U@B_{16}N_{16}$ have more reactivity than $B_{16}N_{16}$, and $U@B_{16}N_{16}$ exhibits greater reactivity than $U@B_{12}N_{12}$ and $Cm@B_{12}N_{12}$. Consequently, the stability of $U@B_{12}N_{12}$, $Cm@B_{12}N_{12}$, and $U@B_{16}N_{16}$ is lower than that of $B_{16}N_{16}$.[8,9] Detailed information on the ionization potential and electron affinity can be found in Part 4 in the Supporting Information. The calculated VIP, AIP, VEA, and AEA values using the BP86 functional are consistent with the discussed results and are listed in Table S4 of the Supporting Information. The lower stability of endohedral metallo-BN fullerenes relative to the BN cage is potentially attributable to the energy level inversion of superatomic orbitals.

CONCLUSIONS

In this study, we investigated the endohedral metallo-BN fullerenes $U@B_{12}N_{12}$, $Cm@B_{12}N_{12}$, and $U@B_{16}N_{16}$ using the first-principles theory. The results show that $U@B_{12}N_{12}$, $Cm@B_{12}N_{12}$, and $U@B_{16}N_{16}$ are superatoms, and their electronic configurations are $1P^61S^21D^{10}1F^{14}2P^62S^22D^{10}2F^{12}3P^6$, $1P^61S^21D^{10}1F^{14}1G^{16}1H^{16}2S^22P^62D^{10}2F^{12}$, and $1P^61S^21D^{10}1F^{14}2P^62S^22D^{10}2F^{14}$, respectively. The superatomic orbitals 1S, 1P, 1D, and 1F originate from the 2s atomic orbitals of BN cages, while 2S, 2P, 2D, 2F, and 3P superatomic orbitals result from the hybridization of the BN cage's 2p orbitals with the 7s, 7p, 6d, and 5f orbitals of the actinide atoms. And the HOMO−LUMO gaps for $U@B_{12}N_{12}$, $Cm@B_{12}N_{12}$, and $U@B_{16}N_{16}$ are 3.32, 1.41, and 0.61 eV, respectively, illustrating that the incorporation of actinide atoms into BN cages significantly reduces the energy gaps. Furthermore, the AIPs for $U@B_{12}N_{12}$, $Cm@B_{12}N_{12}$, $U@B_{16}N_{16}$, and $B_{16}N_{16}$ are 6.68, 6.18, 5.43, and 8.81 eV, while the AEAs are 0.84, 0.83, 1.43, and 0.68 eV, respectively. The analyses of ionization potential and electron affinity suggest that the stabilities of these endohedral metallo-BN fullerenes are lower than that of BN cages, which may be due to the flip of the superatomic MO energy levels. In traditional atoms, active atoms easily undergo chemical reactions with other atoms. Therefore, the reactivity of these superatoms makes them promising candidates for cluster assembly materials while maintaining structural integrity. This investigation sheds light on the properties of endohedral metallo-BN fullerenes from a superatomic perspective.

COMPUTATIONAL METHODS

The Amsterdam density functional package (ADF)[42] was utilized to perform the computations relevant to this study. Within ADF, the geometries were optimized using the generalized gradient approximation exchange−correlation functional PBE.[43] Scalar relativistic effects were accounted for using the zeroth-order regular approximations method.[44−46] Moreover, we also used Becke−Perdew (BP86)[47,48] and hybrid PBE0[49] functionals to ensure our calculation. The relativistic valence triple-ζ slater basis sets with two polarization functions (TZ2P) were used along with the frozen core approximation for the 1s-4f electrons of actinide atoms. Similar calculation methods for actinide atoms are widely used.[50,51] Frequency analyses to determine the nature of the stationary points were conducted at the PBE level without imposing any symmetry constraints on the geometry optimizations.

ASSOCIATED CONTENT

Supporting Information

The Supporting Information is available free of charge at https://pubs.acs.org/doi/10.1021/acsomega.4c04765.

The bond energies; the superatomic MOs and spin density; the HOMO−LUMO gaps calculated by other functionals; the detailed ionization potential and electron affinity; and Cartesian coordinates for $U@B_{12}N_{12}$, $Cm@B_{12}N_{12}$, and $U@B_{16}N_{16}$ structures (PDF)

AUTHOR INFORMATION

Corresponding Author

Jia Wang − *College of Information Technology, Jilin Normal University, Siping 136000, China;* orcid.org/0000-0002-5626-9944; Email: wangjia18@jlnu.edu.cn

Authors

Huanming Zhang − *College of Information Technology, Jilin Normal University, Siping 136000, China*

Meiqi Wang − *College of Information Technology, Jilin Normal University, Siping 136000, China*

Wanyi Zhang − *College of Information Technology, Jilin Normal University, Siping 136000, China*

Complete contact information is available at: https://pubs.acs.org/10.1021/acsomega.4c04765

Notes

The authors declare no competing financial interest.

ACKNOWLEDGMENTS

This work was financially supported by the National Natural Science Foundation of China (grant no. 11947039) and the Education Department of Jilin Province (grant no. JJKH20230510KJ and JJKH20230506KJ).

REFERENCES

(1) Fujii, A.; Umeda, T.; Shirakawa, T.; Akasaka, T.; Yoshino, K. Photocurrent Enhancement in Conducting Polymer Device by Doping with Endohedral Metallofullerene La@C82. *Jpn. J. Appl. Phys.* **2002**, *41* (Part 1, No. 4A), 2254−2255.

(2) Meng, J.; Liang, X.; Chen, X.; Zhao, Y. Biological characterizations of [Gd@C82(OH)22]n nanoparticles as fullerene derivatives for cancer therapy. *Integr. Biol.* **2013**, *5* (1), 43−47.

(3) Chen, C.; Xing, G.; Wang, J.; Zhao, Y.; Li, B.; Tang, J.; Jia, G.; Wang, T.; Sun, J.; Xing, L.; et al. Multihydroxylated [Gd@

$C_{82}(OH)_{22}]_n$ Nanoparticles: Antineoplastic Activity of High Efficiency and Low Toxicity. *Nano Lett.* **2005**, *5* (10), 2050−2057.
(4) Kang, S. G.; Zhou, G.; Yang, P.; Liu, Y.; Sun, B.; Huynh, T.; Meng, H.; Zhao, L.; Xing, G.; Chen, C.; et al. Molecular mechanism of pancreatic tumor metastasis inhibition by Gd@C82(OH)22 and its implication for de novo design of nanomedicine. *Proc. Natl. Acad. Sci. U.S.A.* **2012**, *109* (38), 15431−15436.
(5) Jiang, S.-D.; Wang, B.-W.; Su, G.; Wang, Z.-M.; Gao, S. A Mononuclear Dysprosium Complex Featuring Single-Molecule-Magnet Behavior. *Angew. Chem., Int. Ed.* **2010**, *49* (41), 7448−7451.
(6) Woodruff, D. N.; Winpenny, R. E.; Layfield, R. A. Lanthanide single-molecule magnets. *Chem. Rev.* **2013**, *113* (7), 5110−5148.
(7) Dreiser, J. Molecular lanthanide single-ion magnets: from bulk to submonolayers. *J. Phys.: Condens. Matter* **2015**, *27* (18), 183203.
(8) Dai, X.; Gao, Y.; Jiang, W.; Lei, Y.; Wang, Z. U@C28: the electronic structure induced by the 32-electron principle. *Phys. Chem. Chem. Phys.* **2015**, *17* (36), 23308−23311.
(9) Yu, T.; Gao, Y.; Xu, D.; Wang, Z. Actinide endohedral boron clusters: A closed-shell electronic structure of U@B40. *Nano Res.* **2018**, *11* (1), 354−359.
(10) Kroto, H. W. The stability of the fullerenes Cn, with n = 24, 28, 32, 36, 50, 60 and 70. *Nature* **1987**, *329* (6139), 529−531.
(11) Guo, T.; Diener, M. D.; Chai, Y.; Alford, M. J.; Haufler, R. E.; McClure, S. M.; Ohno, T.; Weaver, J. H.; Scuseria, G. E.; Smalley, R. E. Uranium Stabilization of C_{28}: A Tetravalent Fullerene. *Science* **1992**, *257* (5077), 1661−1664.
(12) Dognon, J.-P.; Clavaguéra, C.; Pyykkö, P. A Predicted Organometallic Series Following a 32-Electron Principle: An@C28 (An = Th, Pa+, U2+, Pu4+). *J. Am. Chem. Soc.* **2009**, *131* (1), 238−243.
(13) Pyykkö, P.; Clavaguéra, C.; Dognon, J.-P. The 32-Electron Principle: A New Magic Number. *Computational Methods in Lanthanide and Actinide Chemistry*; John Wiley & Sons, 2015; pp 401−424.
(14) Dognon, J. P.; Clavaguera, C.; Pyykko, P. Towards a 32-electron principle: Pu@Pb12 and related systems. *Angew. Chem., Int. Ed. Engl.* **2007**, *46* (9), 1427−1430.
(15) Martin, T. P.; Bergmann, T.; Göhlich, H.; Lange, T. Observation of electronic shells and shells of atoms in large Na clusters. *Chem. Phys. Lett.* **1990**, *172* (3−4), 209−213.
(16) Knight, W. D.; Clemenger, K.; de Heer, W. A.; Saunders, W. A.; Chou, M. Y.; Cohen, M. L. Electronic Shell Structure and Abundances of Sodium Clusters. *Phys. Rev. Lett.* **1984**, *52* (24), 2141−2143.
(17) Khanna, S. N.; Jena, P. Atomic clusters: Building blocks for a class of solids. *Phys. Rev. B* **1995**, *51* (19), 13705−13716.
(18) Li, J.; Li, X.; Zhai, H. J.; Wang, L. S. Au20: a tetrahedral cluster. *Science* **2003**, *299* (5608), 864−867.
(19) Jena, P. Beyond the Periodic Table of Elements: The Role of Superatoms. *J. Phys. Chem. Lett.* **2013**, *4* (9), 1432−1442.
(20) Castleman, A. W.; Khanna, S. N. Clusters, Superatoms, and Building Blocks of New Materials. *J. Phys. Chem. C* **2009**, *113* (7), 2664−2675.
(21) Claridge, S. A.; Castleman, A. W., Jr.; Khanna, S. N.; Murray, C. B.; Sen, A.; Weiss, P. S. Cluster-assembled materials. *ACS Nano* **2009**, *3* (2), 244−255.
(22) Wang, J.; Jiang, W. R.; Xie, W. Y.; Wang, J. P.; Wang, Z. G. Superatom-assembly induced transition from insulator to semiconductor: A theoretical study. *Sci. China Mater.* **2019**, *62* (3), 416−422.
(23) Xie, W.; Jiang, W.; Gao, Y.; Wang, J.; Wang, Z. Binding for endohedral-metallofullerene superatoms induced by magnetic coupling. *Chem. Commun.* **2018**, *54* (95), 13383−13386.
(24) Reber, A. C.; Khanna, S. N.; Castleman, A. W., Jr. Superatom compounds, clusters, and assemblies: ultra alkali motifs and architectures. *J. Am. Chem. Soc.* **2007**, *129* (33), 10189−10194.
(25) Zheng, W. J.; Thomas, O. C.; Lippa, T. P.; Xu, S. J.; Bowen, K. H., Jr. The ionic KAl13 molecule: a stepping stone to cluster-assembled materials. *J. Chem. Phys.* **2006**, *124* (14), 144304.
(26) Liu, F.; Mostoller, M.; Kaplan, T.; Khanna, S. N.; Jena, P. Evidence for a new class of solids. First-principles study of K(Al13). *Chem. Phys. Lett.* **1996**, *248* (3−4), 213−217.
(27) Mirkin, C. A.; Brett Caldwell, W. Thin film, fullerene-based materials. *Tetrahedron* **1996**, *52* (14), 5113−5130.
(28) Diederich, F.; Thilgen, C. Covalent fullerene chemistry. *Science* **1996**, *271* (5247), 317−324.
(29) Roy, X.; Lee, C. H.; Crowther, A. C.; Schenck, C. L.; Besara, T.; Lalancette, R. A.; Siegrist, T.; Stephens, P. W.; Brus, L. E.; Kim, P.; et al. Nanoscale atoms in solid-state chemistry. *Science* **2013**, *341* (6142), 157−160.
(30) Feng, M.; Zhao, J.; Petek, H. Atomlike, hollow-core-bound molecular orbitals of C60. *Science* **2008**, *320* (5874), 359−362.
(31) Zhai, H.-J.; Zhao, Y.-F.; Li, W.-L.; Chen, Q.; Bai, H.; Hu, H.-S.; Piazza, Z. A.; Tian, W.-J.; Lu, H.-G.; Wu, Y.-B.; et al. Observation of an all-boron fullerene. *Nat. Chem.* **2014**, *6* (8), 727−731.
(32) Wang, J.; Yu, T.; Gao, Y.; Wang, Z. All-boron fullerene B40: a superatomic structure. *Sci. China Mater.* **2017**, *60* (12), 1264−1268.
(33) Seifert, G.; Fowler, P. W.; Mitchell, D.; Porezag, D.; Frauenheim, T. Boron-nitrogen analogues of the fullerenes: electronic and structural properties. *Chem. Phys. Lett.* **1997**, *268* (5−6), 352−358.
(34) Xie, W.; Wang, J.; Wang, J.; Wu, X.; Wang, Z.; Zhang, R.-Q. High-Angular-Momentum Orbitals and Superatomic Characteristics of Boron-Nitrogen Cages. *J. Phys. Chem. C* **2020**, *124* (6), 3881−3885.
(35) Xia, X.; Jelski, D. A.; Bowser, J. R.; George, T. F. MNDO study of boron-nitrogen analogs of buckminsterfullerene. *J. Am. Chem. Soc.* **1992**, *114* (16), 6493−6496.
(36) Stephan, O.; Bando, Y.; Loiseau, A.; Willaime, F.; Shramchenko, N.; Tamiya, T.; Sato, T. Formation of small single-layer and nested BN cages under electron irradiation of nanotubes and bulk material. *Appl. Phys. A: Mater. Sci. Process.* **1998**, *67* (1), 107−111.
(37) Sun, Q.; Wang, Q.; Jena, P. Storage of Molecular Hydrogen in B−N Cage: Energetics and Thermal Stability. *Nano Lett.* **2005**, *5* (7), 1273−1277.
(38) Paine, R. T.; Narula, C. K. Synthetic routes to boron nitride. *Chem. Rev.* **1990**, *90* (1), 73−91.
(39) Li, R. Y.; Wang, Y. Modification of boron nitride nanocages by titanium doping results unexpectedly in exohedral complexes. *Nat. Commun.* **2019**, *10* (1), 4908.
(40) Parr, R. G. Density Functional Theory. *Annu. Rev. Phys. Chem.* **1983**, *34* (1), 631−656.
(41) Gao, Y.; Wang, B.; Lei, Y. Y.; Teo, B. K.; Wang, Z. G. Actinide-embedded gold superatom models: Electronic structure, spectroscopic properties, and applications in surface-enhanced Raman scattering. *Nano Res.* **2016**, *9* (3), 622−632.
(42) te Velde, G.; Bickelhaupt, F. M.; Baerends, E. J.; Fonseca Guerra, C.; van Gisbergen, S. J. A.; Snijders, J. G.; Ziegler, T. Chemistry with ADF. *J. Comput. Chem.* **2001**, *22* (9), 931−967.
(43) Perdew, J. P.; Burke, K.; Ernzerhof, M. Generalized Gradient Approximation Made Simple. *Phys. Rev. Lett.* **1996**, *77* (18), 3865−3868.
(44) Lenthe, E. v.; Baerends, E. J.; Snijders, J. G. Relativistic regular two-component Hamiltonians. *J. Chem. Phys.* **1993**, *99* (6), 4597−4610.
(45) van Lenthe, E.; Baerends, E. J.; Snijders, J. G. Relativistic total energy using regular approximations. *J. Chem. Phys.* **1994**, *101* (11), 9783−9792.
(46) van Wüllen, C. Molecular density functional calculations in the regular relativistic approximation: Method, application to coinage metal diatomics, hydrides, fluorides and chlorides, and comparison with first-order relativistic calculations. *J. Chem. Phys.* **1998**, *109* (2), 392−399.
(47) Becke, A. D. Density-functional exchange-energy approximation with correct asymptotic behavior. *Phys. Rev. A* **1988**, *38* (6), 3098−3100.

https://doi.org/10.1021/acsomega.4c04765
ACS Omega 2024, 9, 27748−27753

(48) Perdew, J. P. Density-functional approximation for the correlation energy of the inhomogeneous electron gas. *Phys. Rev. B* **1986**, *33* (12), 8822−8824.
(49) Adamo, C.; Barone, V. Toward reliable density functional methods without adjustable parameters: The PBE0 model. *J. Chem. Phys.* **1999**, *110* (13), 6158−6170.
(50) Xie, W. Y.; Zhu, Y.; Wang, J. P.; Cheng, A. H.; Wang, Z. G. Magnetic Coupling Induced Self-Assembly at Atomic Level. *Chin. Phys. Lett.* **2019**, *36* (11), 116401.
(51) Wang, J.; Gong, K.; Lu, F.; Xie, W.; Zhu, Y.; Wang, Z. Electronic Transport Inhibiting of Carbon Nanotubes by 5f Elements. *Adv. Theory Simul.* **2020**, *3* (2), 1900226.

https://doi.org/10.1021/acsomega.4c04765
ACS Omega 2024, 9, 27748−27753